Article

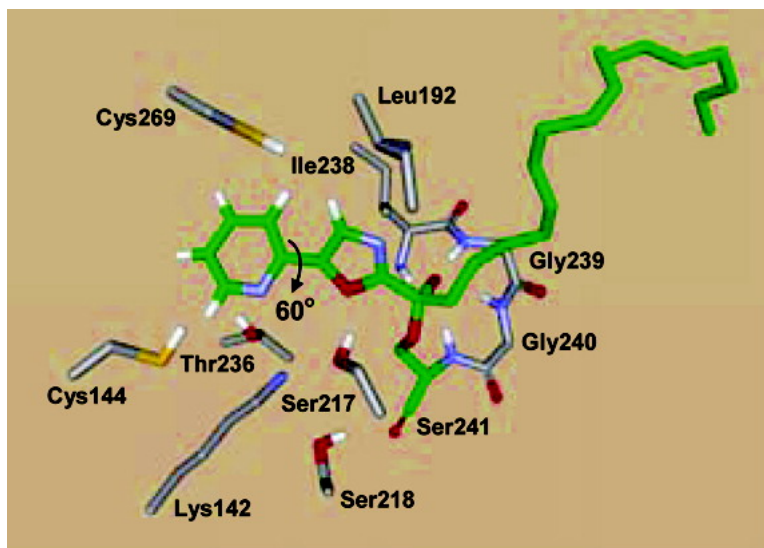# Elucidation of Fatty Acid Amide Hydrolase Inhibition by Potent -Ketoheterocycle Derivatives from Monte Carlo Simulations

Cristiano Ruch Werneck Guimares, Dale L. Boger, and William L. Jorgensen

More About This Article

Additional resources and features associated with this article are available within the HTML version:

- Supporting Information
- Links to the 7 articles that cite this article, as of the time of this article download
- Access to high resolution figures
- Links to articles and content related to this article
- Copyright permission to reproduce figures and/or text from this article

View the Full Text HTML

Elucidation of Fatty Acid Amide Hydrolase Inhibition by Potent α-Ketoheterocycle Derivatives from Monte Carlo Simulations

Cristiano Ruch Werneck Guimarães,[†] Dale L. Boger,[‡] and William L. Jorgensen*,[†]

Contribution from the Department of Chemistry, Yale University, 225 Prospect Street, New Haven, Connecticut 06520-8107, and Department of Chemistry and the Skaggs Institute for Chemical Biology, The Scripps Research Institute, 10550 North Torrey Pines Road, La Jolla, California 92037

Received August 9, 2005; E-mail: william.jorgensen@yale.edu

Abstract: Fatty acid amide hydrolase (FAAH) is a serine hydrolase responsible for the degradation of anandamide, an endogenous cannabinoid agonist, and oleamide, a sleep-inducing lipid. Recently, Boger and co-workers reported a potent, selective, and efficacious class of reversible α-ketoheterocycle inhibitors of FAAH that produce analgesia in animal models (*J. Med. Chem.* **2005**, *48,* 1849−1856; *Bioorg. Med. Chem. Lett.* **2005**, *15*, 1423−1428). Key aspects of the structure−activity data are addressed here through computational analysis of FAAH inhibition using Monte Carlo (MC) simulations in conjunction with free energy perturbation (FEP) calculations. The MC/FEP simulations demonstrate that incorporation of pyridine at the C5 position of the 2-keto-oxazole and 2-keto-1,3,4-oxadiazole derivatives significantly enhances binding affinity by formation of a hydrogen-bonded array between the pyridyl nitrogen and Lys142 and Thr236. The results also attribute the activity boost upon substitution of oxazole by oxadiazole to reduced steric interactions in the active site and a lower torsional energy penalty upon binding.

Introduction

Fatty acid amide hydrolase (FAAH)[1−3] is an integral membrane protein responsible for the degradation of fatty acid primary amides and ethanolamides such as anandamide and oleamide (Scheme 1).[4,5] Anandamide binds and activates the central (CB1) and peripheral (CB2) cannabinoid receptors as well as the vanilloid receptor (VR1) through which it is thought to exert its analgesic and cannabinoid effects.[6−9] Like the cannabinoids, anandamide exhibits behavioral analgesia suppressing neurotransmission[10] and anxiolytic, antiemetic, appetite enhancement, and antiproliferative activity. It also displays neuroprotective effects that have clinical implications in the

Scheme 1
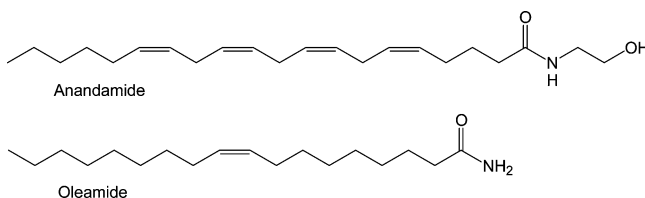
treatment of sleep disorders, anxiety, epilepsy, cachexia, cancer, and neurodegenerative disorders.[6,7,11] Oleamide was found to accumulate in the cerebrospinal fluid under conditions of sleep deprivation and to induce physiological sleep in animals; it reduced mobility, shortened the sleep induction period, and lengthened the time spent in slow wave sleep 2 at the expense of wakening without the side effects of sedatives and hypnotics and the suicide-abuse potential of such central nervous system depressants.[12,13]

Serine hydrolases represent one of the largest classes of enzymes including serine proteases, lipases, esterases, amidases, and transacetylases. FAAH constitutes the only characterized mammalian member of a class of serine hydrolases (amidase signature family) that bear a unique catalytic triad (Ser-Ser-Lys).[14,15] Due to its unique mammalian distribution, its selectively targetable active site and catalytic mechanism, and the
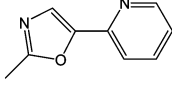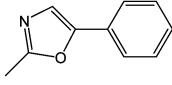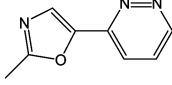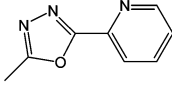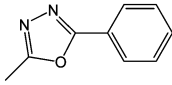
† Yale University.

‡ The Scripps Research Institute.

(1) Cravatt, B. F.; Giang, D. K.; Mayfield, S. P.; Boger, D. L.; Lerner, R. A.; Gilula, N. B. *Nature (London)* **1996**, *384*, 83−87.

(2) Giang, D. K.; Cravatt, B. F. *Proc. Natl. Acad. Sci. U.S.A.* **1997**, *94*, 2238−2242.

(3) Patricelli, M. P.; Cravatt, B. F. *Vit. Hormones* **2001**, *62*, 95−131.

(4) Boger, D. L.; Fecik, R. A.; Patterson, J. E.; Miyauchi, H.; Patricelli, M. P.; Cravatt, B. F. *Bioorg. Med. Chem. Lett.* **2000**, *10*, 2613−2616.

(5) Lang, W.; Qin, C.; Lin, S.; Khanolkar, A. D.; Goutopoulos, A.; Fan, P.; Abouzid, K.; Meng, Z.; Biegel, D.; Makriyannis, A. *J. Med. Chem.* **1999**, *42*, 896−902.

(6) Martin, B. R.; Mechoulam, R.; Razdan, R. K. *Life Sci.* **1999**, *65*, 573−595.

(7) Axelrod, J.; Felder, C. C. *Neurochem. Res.* **1998**, *23*, 575−581.

(8) Zygmunt, P. M.; Petersson, J.; Andersson, D. A.; Chuang, H.; Sorgard, M.; Di Marzo, V.; Julius, D.; Hogestatt, E. D. *Nature (London)* **1999**, *400*, 452−457.

(9) Smart, D.; Gunthorpe, M. J.; Jerman, J. C.; Nasir, S.; Gray, J.; Muir, A. I.; Chambers, J. K.; Randall, A. D.; Davis, J. B. *Br. J. Pharmacol.* **2000**, *129*, 227−230.

(10) Walker, J. M.; Huang, S. M.; Strangman, N. M.; Tsou, K.; Sanudo-Pena, M. C. *Proc. Natl. Acad. Sci. U.S.A.* **1999**, *96*, 12198−12203.

(11) Di Marzo, V.; Bisogno, T.; De Petrocellis, L.; Melck, D.; Martin, B. R. *Curr. Med. Chem.* **1999**, *6*, 721−744.

(12) Cravatt, B. F.; Prospero-Garcia, O.; Suizdak, G.; Gilula, N. B.; Henriksen, S. J.; Boger, D. L.; Lerner, R. A. *Science* **1995**, *268*, 1506−1509.

(13) Huitron-Resendiz, S.; Gombart, L.; Cravatt, B. F.; Henriksen, S. J. *Exp. Neurol.* **2001**, *172*, 235−243.
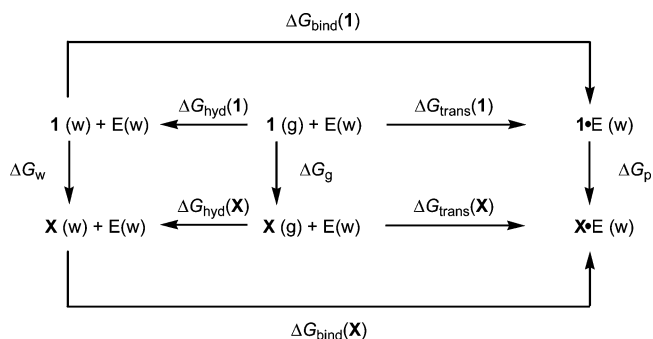
Table 1. Selected Substituted α-Keto Oxazole and Oxadiazole Inhibitors of FAAH

Compound	R	K_i (μM)[a]
1		0.018
2		0.32
3		0.014
4		0.003
5		0.016

[a] References 17, 18.

ramifications of its inactivation, increased endogenous levels of anandamide and oleamide, FAAH has emerged as a potential new therapeutic target for pain management and sleep disorders.[16]

In recent studies, a potent, selective, and efficacious class of reversible α-ketoheterocycle inhibitors of FAAH has been reported.[17,18] Here, to understand key aspects of the structure–activity data, a computational analysis of the FAAH inhibition has been conducted using Monte Carlo (MC)[19] simulations in conjunction with free energy perturbation (FEP) calculations.[20–23] More specifically, relative free energies of binding to FAAH are computed for the compounds in Table 1 and compared to experimental inhibition data; all compounds, although reversible inhibitors, are covalently bound to the enzyme with the electrophilic carbonyl group attacked by Ser241 of the catalytic triad. There are clearly profound effects on activity associated with introduction of nitrogens into the α-ketoheterocycles that warrant investigation. Thus, the quantitative binding results are accompanied by extensive analyses of the computed structures for the FAAH-inhibitor complexes. In addition, to verify the

(14) Bracey, M. H.; Hansen, M.; Masuda, K.; Stevens, R. C.; Cravatt, B. F. *Science* **2002**, *298*, 1793–1796.
(15) McKinney, M. K.; Cravatt, B. F. *J. Biol. Chem.* **2003**, *278*, 37393–37399.
(16) Cravatt, B. F.; Lichtman, A. H. *Curr. Opin. Chem. Biol.* **2003**, *7*, 469–475.
(17) Boger, D. L.; Miyauchi, H.; Du, W.; Hardouin, C.; Fecik, R. A.; Cheng, H.; Hwang, I.; Hedrick, M. P.; Leung, D.; Acevedo, O.; Guimarães, C. R. W.; Jorgensen, W. L.; Cravatt, B. F. *J. Med. Chem.* **2005**, *48*, 1849–1856.
(18) Leung, D.; Du, W.; Hardouin, C.; Cheng, H.; Hwang, I.; Cravatt, B. F.; Boger, D. L. *Bioorg. Med. Chem. Lett.* **2005**, *15*, 1423–1428.
(19) Allen, M. P.; Tildesley, D. J. *Computer Simulations of Liquids*; Clarendon Press: Oxford, U.K., 1987.
(20) Zwanzig, R. *J. Chem. Phys.* **1954**, *22*, 1420–1426.
(21) Jorgensen, W. L.; Ravimohan, C. *J. Chem. Phys.* **1985**, *83*, 3050–3056.
(22) Jorgensen, W. L. *Acc. Chem. Res.* **1989**, *22*, 184–189.
(23) Kollman, P. A. *Chem. Rev.* **1993**, *93*, 2395–2417.

Figure 1. Thermodynamic cycles used for the calculation of relative free energies. ΔG_{hyd}, ΔG_{trans}, and ΔG_{bind} are the absolute free energies of hydration, transfer from the gas phase to the covalent complex, and binding. ΔG_g, ΔG_w, and ΔG_p are the free energy changes for the transformation of **1** into any other compound **X** in the gas phase, water, and protein.

influence of hydration on the binding process, the relative free energies of hydration for the inhibitors were calculated.

Computational Details

Free Energy Changes. When calculating relative free energies, thermodynamic cycles are generally applied.[24] The ones used here are illustrated in Figure 1. Since free energy is a thermodynamic state function, the cycle on the left side of Figure 1 gives the relative free energies of hydration (eq 1), where **1** is the 2-pyridyl oxazolyl derivative and **X** is any of the other compounds, ΔG_{hyd} is the absolute free energy of hydration, and $\Delta G_w(1 \rightarrow X)$ and $\Delta G_g(1 \rightarrow X)$ are the free energies associated with the transformation of **1** into **X** in water and in the gas phase.

$$\Delta\Delta G_{hyd} = \Delta G_{hyd}(X) - \Delta G_{hyd}(1)$$
$$= \Delta G_w(1 \rightarrow X) - \Delta G_g(1 \rightarrow X) \quad (1)$$

The cycle on the right side of Figure 1 gives the relative free energies of transfer from the gas phase to the covalent complex in water between **1** and **X** (eq 2), where ΔG_{trans} is the absolute free energy of transfer, and $\Delta G_p(1 \rightarrow X)$ is the free energy associated with the transformation of **1** into **X** in the enzymatic environment.

$$\Delta\Delta G_{trans} = \Delta G_{trans}(X) - \Delta G_{trans}(1)$$
$$= \Delta G_p(1 \rightarrow X) - \Delta G_g(1 \rightarrow X) \quad (2)$$

Finally, the external cycle of Figure 1 gives the relative free energies of covalent binding to FAAH (eq 3), where ΔG_{bind} is the absolute free energy of binding.

$$\Delta\Delta G_{bind} = \Delta G_{bind}(X) - \Delta G_{bind}(1)$$
$$= \Delta G_p(1 \rightarrow X) - \Delta G_w(1 \rightarrow X) \quad (3)$$

It should also be noted that $\Delta\Delta G_{bind}$ can be rewritten as the difference between $\Delta\Delta G_{trans}$ and $\Delta\Delta G_{hyd}$ (eq 4). In this manner, the binding process is separated into dehydration and transfer from the gas phase to the covalent complex; this facilitates the rationalization of the activity order. The required $\Delta G(1 \rightarrow X)$ terms are computed by transforming **1** into **X** in the different

(24) Wong, C. F.; McCammon, J. A. *J. Am. Chem. Soc.* **1986**, *108*, 3830–3832.

environments through the FEP methodology.[21]

$$\Delta\Delta G_{\text{bind}} = \Delta\Delta G_{\text{trans}} - \Delta\Delta G_{\text{hyd}}$$
$$= \Delta G_{\text{p}}(\mathbf{1} \rightarrow \mathbf{X}) - \Delta G_{\text{w}}(\mathbf{1} \rightarrow \mathbf{X}) \quad\quad (4)$$

Protein-Inhibitor Complexes. Cartesian coordinates for the 2.8 Å FAAH crystal structure complexed to methoxyarachidonyl phosphonate (MAP) (Brookhaven Protein Data Bank code 1mt5) were employed.[25] From the dimeric enzyme, only one active site was retained and taken as the center of the system. Residues with any atom within 15 Å from the center were retained in the simulations and any clipped residues were capped with acetyl or *N*-methylamine groups. The MAP inhibitor was removed, and using the BOMB program,[26] **1** was inserted and subsequently covalently bound to Ser241. The enzymatic system then has 2677 atoms, consisting of 167 amino acid residues plus the inhibitor. Following conjugate-gradient minimizations, degrees of freedom for the protein backbone atoms were not sampled in the MC simulations. Only the bond angles and dihedral angles for the side chains of residues with any atom within 10 Å from the center of the system were varied; however, the inhibitors are fully flexible in the MC simulations except as specified below.

Partial atomic charges totaling −1 e were computed for all inhibitors covalently bound to Ser241 using the CM1A procedure.[27] Charge neutrality was imposed by having a total protein charge of +1 e; charged residues near the active site were assigned normal protonation states at physiological pH, and the adjustments for neutrality were made to the most distant residues. The entire system was solvated with a 22-Å radius water cap consisting of 603 molecules, and a half-harmonic potential with a force constant of 1.5 kcal/mol·Å² was applied to water molecules at distances greater than 22 Å from the center of the system to discourage evaporation. The preparation of the enzymatic system was much facilitated by use of the Chop delegate and MidasPlus 2.1.[28]

As discussed previously,[29] the use of a spherical cap of water rather than periodic boundary conditions affects the calculated free energies of hydration in simple systems. Therefore, to cancel any potential errors, a 22-Å water cap was also used for the unbound perturbations for $\mathbf{1} \rightarrow \mathbf{X}$ yielding $\Delta G_{\text{w}}(\mathbf{1} \rightarrow \mathbf{X})$. In this case, the inhibitors were neutral and the partial atomic charges were again obtained from the CM1A procedure.[27]

MC Simulations. The $\mathbf{1} \rightarrow \mathbf{X}$ transformations in all environments were performed using the single topology approach by melding the force field parameters for bond lengths, bond angles, torsions, and nonbonded interactions.[21] To keep the number of atoms fixed, dummy atoms (DM) were introduced for hydrogens which exist in one state and have no counterpart in the other. Bond lengths for transformations requiring annihilation or creation of a hydrogen were not sampled; the C−H distances were perturbed from 1.08 to 0.5 Å for the N−DM distances. Shrinking the bond length for dummy atoms is a common

practice to improve convergence in FEP simulations.[21,30−32] The bond angles involving dummy atoms have the same parameters as their counterparts in the other state. Associated unphysical contributions to the free-energy differences cancel in a thermodynamic cycle.[30,32]

The MC/FEP calculations for the $\mathbf{1} \rightarrow \mathbf{X}$ transformations were executed at 25 °C using double-wide sampling.[21] The initial and final states were coupled using 20 windows with values for the coupling parameter (λ) evenly distributed between 0 and 1 (0.025, 0.075, ..., 0.925, 0.975). Initial relaxation of the solvent was performed for 5×10^6 configurations, followed by 30×10^6 configurations of full equilibration and 100×10^6 configurations of averaging for each window. For the gas-phase simulations, 20×10^6 configurations of equilibration and 40×10^6 configurations of averaging were employed for each window. These are all long MC runs by normal standards. The structures that are presented here are averages of 100 individual structures obtained during the averaging periods for the 0.025 window for **1** and 0.975 window for **2−5**.

MCPRO 1.68 was used to perform all MC calculations.[33] Established procedures including Metropolis and preferential sampling were employed, and statistical uncertainties were obtained from the batch means procedure with batch sizes of 1 $\times$ 10^6 configurations.[19] Attempted moves of the covalent complexes and inhibitors in water occurred every 10 configurations. The TIP4P model[34] was used for water and the covalent complexes were represented with the OPLS-AA force field,[35] with the exception of the CM1A atomic charges for the inhibitors. Finally, residue-based cutoffs of 10 Å were employed.

Results and Discussion

Conformational Preference for 1. In a recent study, a model for **1** bound covalently to FAAH was proposed from MC simulations, and key interactions were noted.[17] The average structure that emerged (Figure 2) features an extensive hydrogen-bonded network between the enzyme and the pyridyl nitrogen and oxazolyl oxygen of **1**. Specifically, the oxazolyl oxygen is hydrogen bonded to the hydroxyl group of Ser217 of the catalytic triad, which accepts a hydrogen bond from the protonated nitrogen of Lys142, also from the catalytic triad. The ammonium group of this residue donates hydrogen bonds to the pyridyl nitrogen of **1**, and to the hydroxyl groups of Ser218 and Thr236. An additional hydrogen bond is formed between the pyridyl nitrogen of **1** and the hydroxyl group of Thr236. The oxazolyl nitrogen of **1** does not form any hydrogen bonds with the enzyme or water. Regarding the interactions for the oxyanion, formed by the attack of the Ser241 side-chain oxygen on the carbonyl group of **1**, the negatively charged oxygen is hydrogen bonded to the backbone nitrogens of Ile238, Gly239, Gly240, and Ser241. The lipid chain of **1** is surrounded by numerous hydrophobic and aromatic residues including Leu192, Phe194, Tyr335, Leu372, Ala377, Leu380, Phe381, Leu404, Phe432, Thr488, Ile491, Val495, and Trp531.[17]

(25) Bracey, M. H.; Hanson, M. A.; Masuda, M. A.; Stevens, R. C.; Cravatt, B. F. *Science* **2002**, *298*, 1793−1796.
(26) Jorgensen, W. L. *BOMB, Version 2.5*; Yale University: New Haven, CT, 2005.
(27) Storer, J. W.; Giesen, D. J.; Cramer, C. J.; Truhlar, D. G. *J. Comput-Aided Mol. Design* **1995**, *9*, 87−110.
(28) (a) Tirado-Rives, J. *Chop*; Yale University: New Haven, CT, 2002. (b) Huang, C.; Pettersen, E.; Couch, G.; Ferrin, T. *MidasPlus 2.1*; University of California: San Francisco, CA, 1994.
(29) Essex, J.; Jorgensen, W. L. *J. Comput. Chem.* **1995**, *16*, 9510−972.

(30) Boresch, S.; Karplus, M. *J. Phys. Chem. A* **1999**, *103*, 103−118.
(31) Pearlman, D. A.; Kollman, P. A. J. Chem. Phys. **1991**, *94*, 4532−4545.
(32) Price, D. J.; Jorgensen, W. L. *J. Comput-Aided Mol. Design* **2001**, *15*, 681−695.
(33) Jorgensen, W. L.; Tirado-Rives, J. *J. Comput. Chem.* **2005**, *26*, 1689−1700.
(34) Jorgensen, W. L.; Chandrasekhar, J.; Madura, J. D.; Impey, W.; Klein, M. L. *J. Chem. Phys.* **1983**, *79*, 926−935.
(35) Jorgensen, W. L.; Maxwell, D. S.; Tirado-Rives, J. *J. Am. Chem. Soc.* **1996**, *118*, 11225−11236.
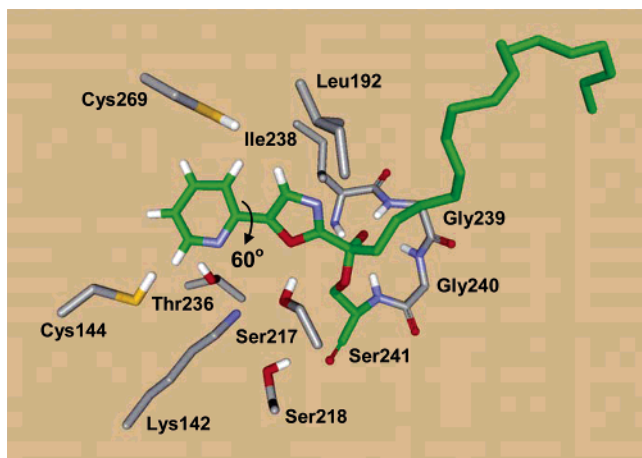
Figure 2. Average structure from an MC simulation illustrating hydrogen-bonding interactions between **1** and FAAH. Hydrogens of Lys142 are not shown for clarity.

The value of the NCCO dihedral angle connecting the two rings is ca. 60° (Figure 2), when **1** is bound to FAAH. As **1** is the reference state for the FEP simulations in all environments, it is also important to determine the underlying conformational preference in water and the gas phase. Thus, the OPLS/CM1A force field was tested, the torsional energy profile for NCCO in the model compound, 5-(2-pyridyl)-oxazole, was obtained, and the results were compared to those from DFT calculations at the B3LYP/6-31G(d) level.[36] Figure 3 illustrates the good agreement between the two levels of theory. Both find the energy minimum with a 180° dihedral angle to be significantly more stable than the 0° alternative in the gas phase; 3.5 kcal/mol more stable with OPLS/CM1A and 2.6 kcal/mol with B3LYP. Thus, the intrinsic preference is for the oxazolyl oxygen and pyridyl nitrogen to be anti.

After validating the force field for this system, MC/FEP calculations were carried out to obtain the torsional free-energy profile for the NCCO angle of **1** in TIP4P water; a 22-Å water cap with 1476 water molecules was used. The free-energy curve (Figure 4) was obtained using increments of 10°. Initial relaxation of the solvent was performed for 5×10^6 configurations. This was followed by 20×10^6 configurations of full equilibration and 80×10^6 configurations of averaging for each window using double-wide sampling.[21] Figure 4 shows that while the barrier in water is unaltered from the gas phase, the difference between the two minima is reduced from 3.5 to 1.7 kcal/mol. More favorable electrostatic interactions with the solvent occur for **1** with the NCCO angle near 0° as the average dipole moment is 5.49 D compared to 4.42 D for the anti conformation. Also, the pyridyl nitrogen and oxazolyl oxygen of syn **1** are less sterically encumbered by opposing CH bonds and more available to form hydrogen bonds to the solvent. However, this additional stabilization is not enough to offset the gas-phase energy difference. The NCCO preference remains anti in water, and the change to 60° in the FAAH complex is driven by development of the hydrogen-bonding network with Ser217, Lys142, and Thr236 (Figure 2). Additional MC simulations were initiated with the pyridyl ring of **1** flipped; the resultant intermolecular energies were always higher and the systems reverted to the illustrated conformation for **1** with the
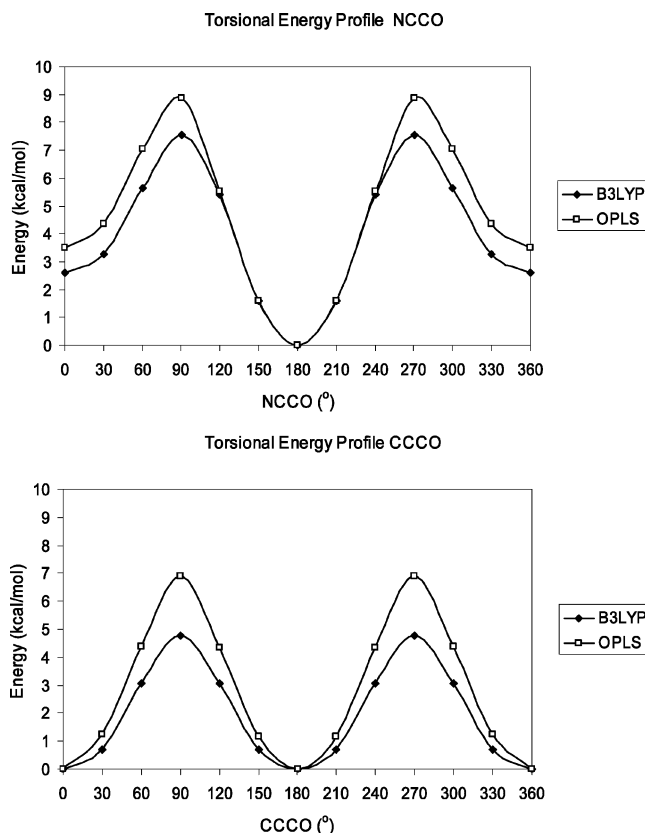
(36) Frisch, M. J.; et al. *Gaussian 98*, revision A.9; Gaussian, Inc.: Pittsburgh, PA, 1998.

Figure 3. Inter-ring torsional energy profiles in the gas phase for the NCCO angle in 5-(2-pyridyl)-oxazole and CCCO angle in 5-phenyl-oxazole using the OPLS/CM1A force field and DFT calculations at the B3LYP/6-31G(d) level.
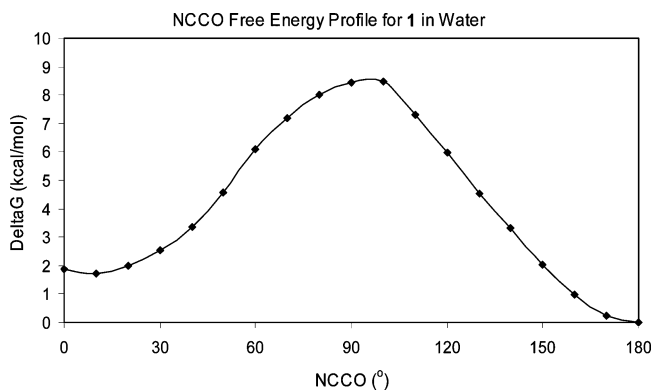

Figure 4. Torsional free-energy profile for the NCCO angle of **1** in water from MC/FEP simulations.

NCCO angle near 60°. Note that the oxazole ring cannot flip without engendering severe steric clashes between FAAH and the aryl group on C5. Consistently, the 4,5-bisphenyl-oxazolyl derivative is completely inactive.[17]

Contributions to Binding. The preferred conformations for **1** in the gas phase, water, and the covalent complex were used in the starting structures for the **1 → X** transformations. Long MC/FEP simulations were performed generating smooth free-energy curves for the **1 → X** conversions in all environments (Figure 5). The resultant free energy differences are reported in Table 2. As noted above (eqs 1−4), the binding process may be decomposed into dehydration and transfer from the gas phase to the protein. The $\Delta\Delta G_{hyd}$ values show that the compounds **1**, **3**, and **4** have similar free energies of hydration. As expected,
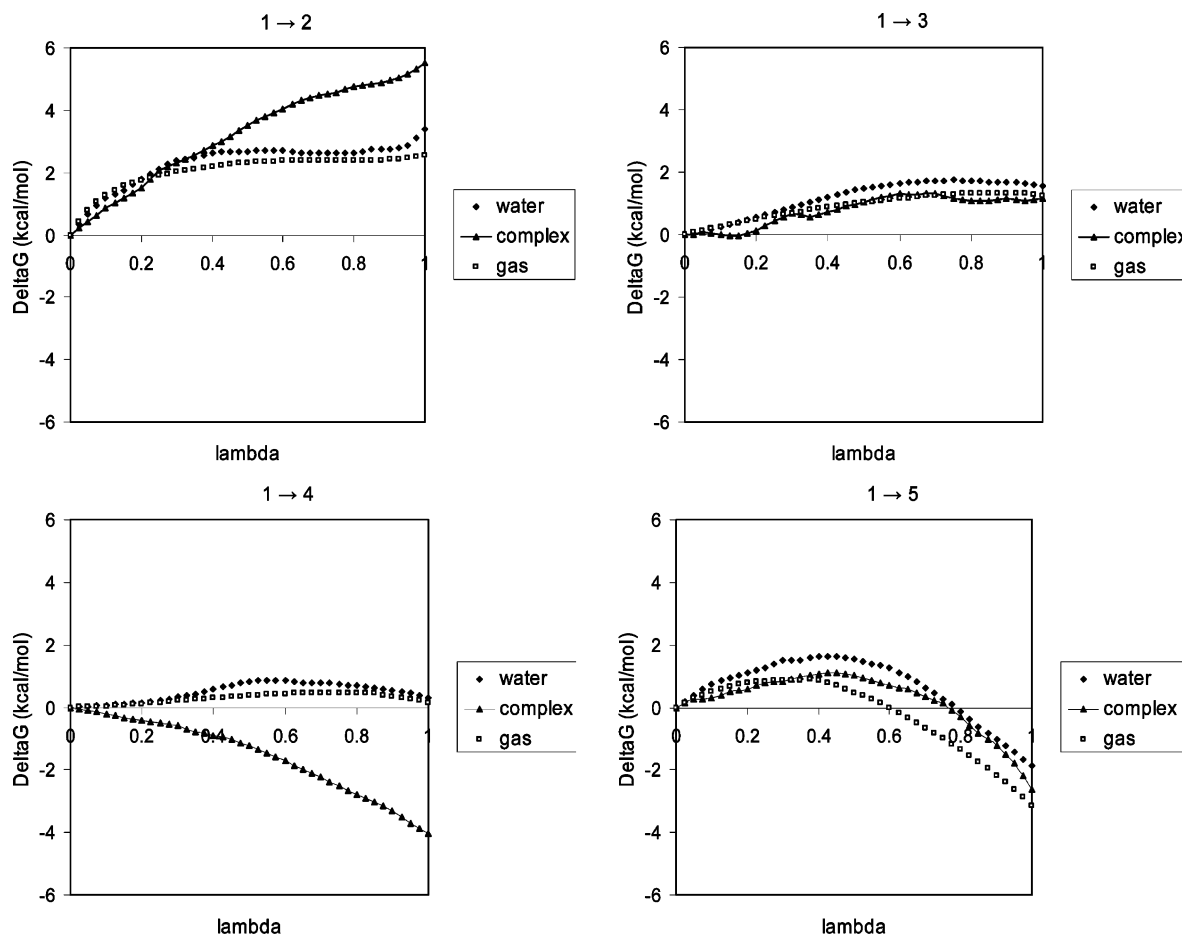
Figure 5. Free-energy curves obtained in the gas phase, water and the covalent complex for all transformations.

Table 2. Free-Energy Differences in the Gas Phase, Water, and the Covalent Complex[a]

	1→2	1→3	1→4	1→5
ΔG_g	2.6 ± 0.0	1.3 ± 0.0	0.2 ± 0.0	-3.0 ± 0.0
ΔG_w	3.4 ± 0.1	1.6 ± 0.0	0.4 ± 0.0	-2.0 ± 0.1
ΔG_p	5.5 ± 0.1	1.2 ± 0.1	-4.0 ± 0.1	-2.6 ± 0.1
$\Delta\Delta G_{hyd}$[b]	0.8 ± 0.1	0.3 ± 0.0	0.2 ± 0.0	1.0 ± 0.1
$\Delta\Delta G_{trans}$[b]	2.9 ± 0.1	-0.1 ± 0.1	-4.2 ± 0.1	0.4 ± 0.1
$\Delta\Delta G_{bind}$[b]	2.1 ± 0.1	-0.4 ± 0.1	-4.4 ± 0.1	-0.6 ± 0.1
$\Delta\Delta G_{bind}$ (exp)[c]	1.7	-0.2	-1.1	-0.1

[a] Values in kcal/mol. Uncertainties in the computed ΔG values obtained from the batch means procedure (ref 19). [b] See eqs 1−3. [c] Based on the K_i data in Table 1 (refs 17, 18).

the phenyl substituted derivatives **2** and **5** are less well hydrated with computed differences of ca. 1 kcal/mol. The results indicate that the introduction of a second nitrogen atom in either the pyridine or oxazole rings generating pyridazine and oxadiazole provides negligible dehydration penalties. Despite the extra hydrogen bond acceptor site for the pyridazine and oxadiazole, the charges on the nitrogens of these rings are significantly less negative than the charges on the pyridyl and oxazolyl nitrogens, and weaker hydrogen bonds with the solvent are formed. For example, the CM1A charge for the oxazolyl nitrogen in unbound **1** is −0.26 e, while the charges for oxazolyl N3 and N4 in **4** are −0.10 and −0.08 e.

Additional important insights can be extracted from the $\Delta\Delta G_{trans}$ values (Table 2) and the average structures displayed in Figure 6. Incorporation of pyridine at the C5 position of the

oxazole and oxadiazole rings significantly enhances the transfer from the gas phase to the protein $\mathbf{2} \rightarrow \mathbf{1}$ (−2.9 kcal/mol) and $\mathbf{5} \rightarrow \mathbf{4}$ (−4.6 kcal/mol). This can be largely attributed to the introduction of the hydrogen-bond interactions between the pyridyl nitrogen and Lys142 and Thr236, which are absent for phenyl. The results also indicate that the substitution of pyridine by pyridazine ($\mathbf{1} \rightarrow \mathbf{3}$) has no effect on the transfer from the gas phase to the protein; as found above, the extra hydrogen-bond acceptor site in pyridazine is counterbalanced by reduced partial negative charges on the nitrogens of this ring. Table 2 also reveals that the transfer from the gas phase to the protein for the 2-keto-1,3,4-oxadiazoles is more favorable than that of the corresponding 2-keto-oxazoles, $\mathbf{1} \rightarrow \mathbf{4}$ (−4.2 kcal/mol) and $\mathbf{2} \rightarrow \mathbf{5}$ (−2.5 kcal/mol). This is not associated with the formation of new hydrogen bonds with the additional nitrogen in the oxadiazole rings (Figure 6). Instead, the more favorable ΔG_{trans} values for **4** and **5** compared to **1** and **2** may be attributed to reduced repulsive interactions between the oxadiazole ring and Ile238. This is apparent in computed residue−residue energy components, and the repulsion between the oxazolyl hydrogen and the methyl group of Ile238 also causes a conformational change for the oxazoles relative to the oxadiazoles. As can be seen in Figure 7, the dihedral angle connecting the two aromatic rings is more out-of-plane for the oxazole derivatives with the oxazolyl C−H twisting away from Ile238.

Intramolecular Contributions to Binding. The different conformations for the oxazole and oxadiazole derivatives in the
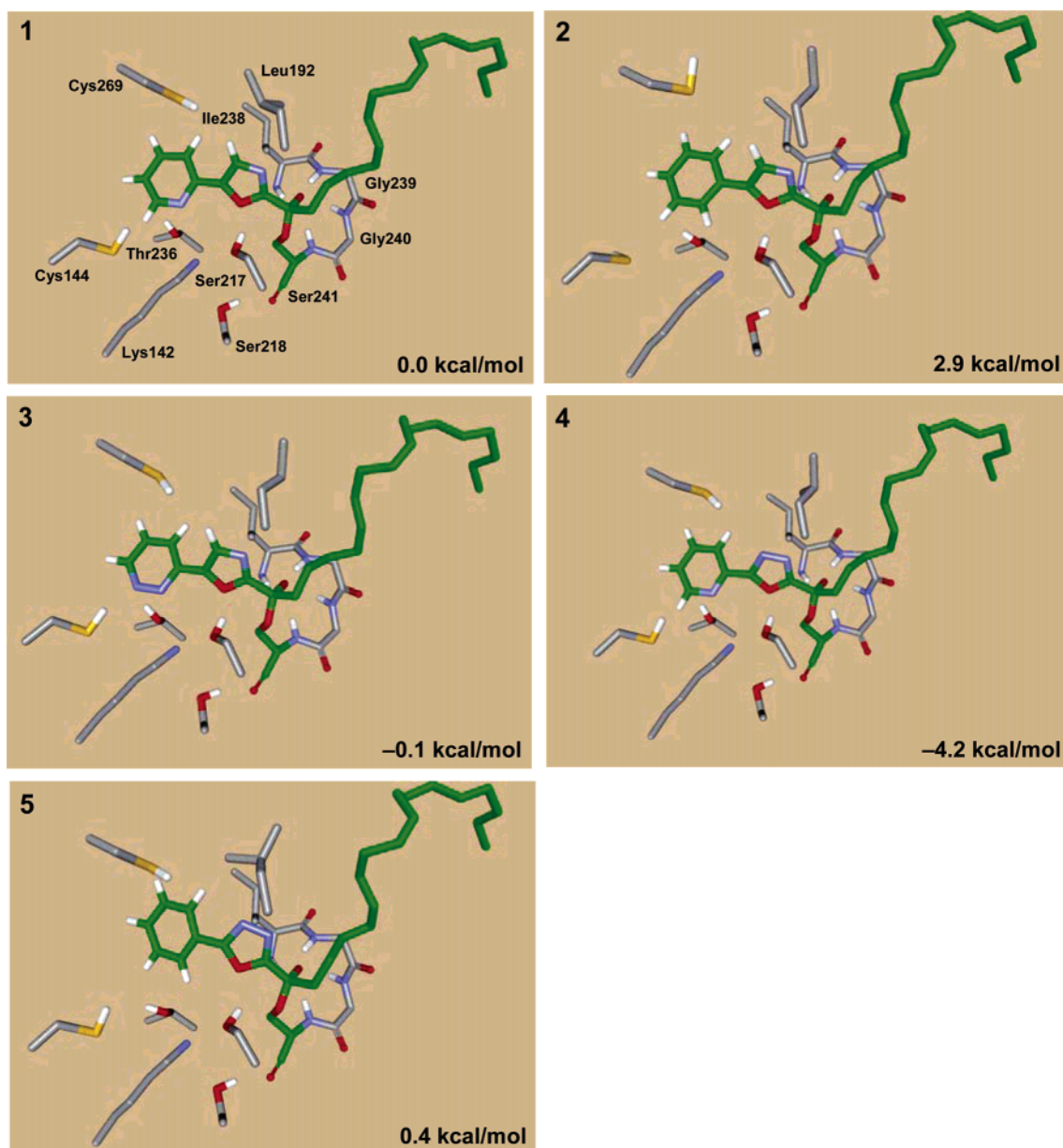
Figure 6. Average structures for the covalent complexes between FAAH and **1**–**5**, and the corresponding $\Delta\Delta G_{\text{trans}}$ values.

covalent complexes with FAAH indicate that the intramolecular contributions to the binding process are variable. Quantitative analysis here needs to be cognizant of the somewhat exaggerated energy-profiles provided by OPLS/CM1A for the dihedral angle connecting the biaryl systems, NCCO for **1**, **3** and **4**, and CCCO for **2** and **5**. This is illustrated in Figure 3 for the NCCO angle in the model compound for **1**, 5-(2-pyridyl)-oxazole, and for the CCCO angle in the model compound for **2**, 5-phenyl-1,3-oxazole. Nevertheless, an estimate of the strain energies involved can be obtained from the probability distributions for the NCCO and CCCO angles, which were obtained from the MC simulations for the five inhibitors in the three environments.

The probability distributions for the XCCO angle in water (Figure 8) and in the gas phase (not shown) all center near 180°, and they are very similar for all compounds. This suggests a negligible intramolecular contribution associated with this degree of freedom upon dehydration of each compound. However, the probability distributions for the XCCO angles in the protein

complexes are centered near 60° for the oxazole derivatives and near 35° and 20° for **4** and **5**, as also reflected in Figure 7. These results, combined with the energy profiles for the XCCO angles in the gas phase, suggest that the oxadiazoles **4** and **5** have the lowest torsional-energy penalty upon transfer from the gas phase to the covalent complex, and consequently upon binding, followed by **2**, **3**, and **1**. The penalty for **1** and **3** likely reduces their binding affinities by 1–2 kcal/mol.

Final Binding Order. The above results provide clear insights into the variations in inhibition of FAAH by **1**–**5**. The analysis focused on the binding differentials provided by hydration of the inhibitors, their accommodation in the active site, and conformational reorganization for the inhibitors upon binding. The key effects are as follows: (1) introduction of the 2-pyridyl nitrogen in going from **2** → **1** and **5** → **4** greatly enhances the binding affinity through hydrogen bonding with Lys142 and Thr236; (2) addition of another nitrogen in going from **1** → **3** has little effect on any of the three binding
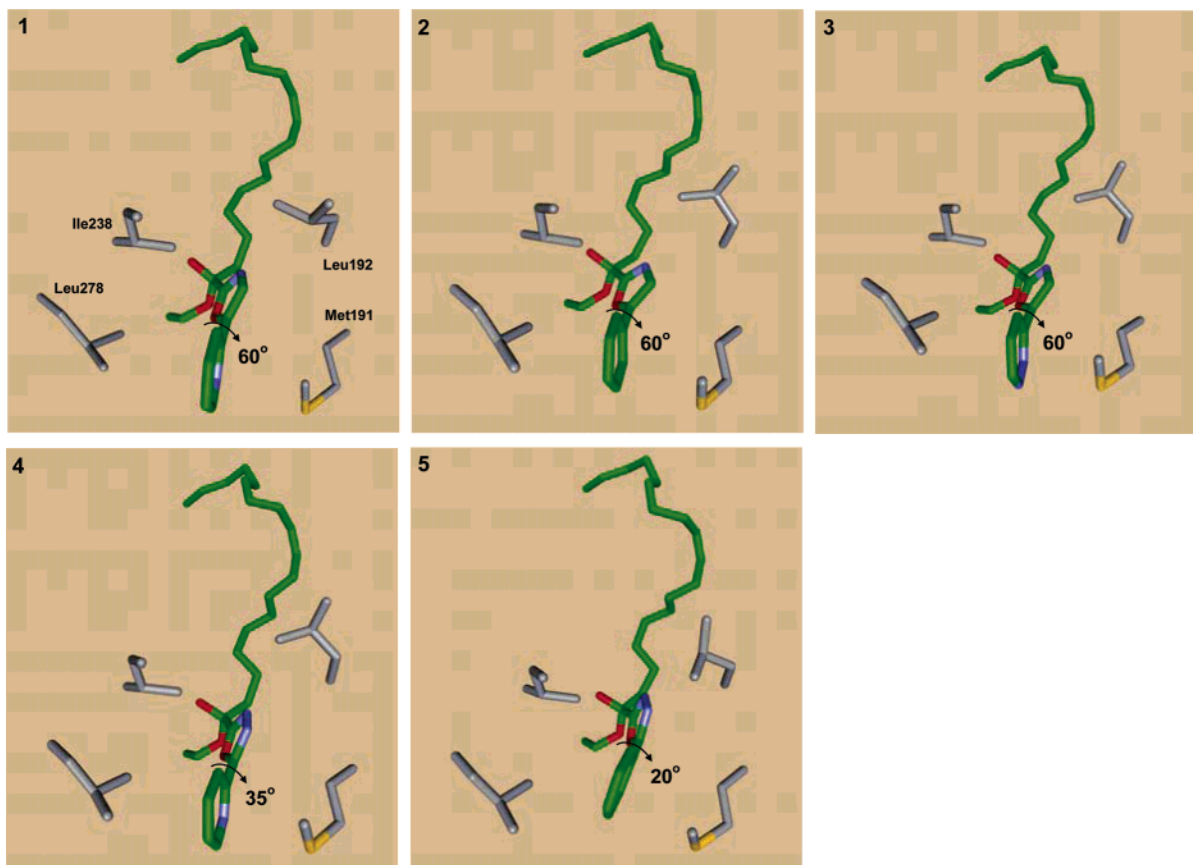
Figure 7. Different view of the average structures for the covalent complexes between FAAH and **1**−**5** illustrating the conformational change for the oxazole (top) and oxadiazole (bottom) derivatives.

components owing to compensation between the additional hydrogen-bonding site and charge delocalization between the two pyridazinyl nitrogens; and (3) the enhanced activity of the oxadiazoles over the oxazoles, **2** → **5** and **1** → **4**, stems from a reduced conformational reorganization penalty for the oxadiazoles and removal of the steric clash between Ile238 and the oxazolyl CH group. Comparison of **1** and **5** is also interesting. Their similar K_i values result from cancellation of the benefit of the pyridyl nitrogen in **1** by the poorer hydration of unbound **5** (1.0 kcal/mol in Table 2), the lack of oxazolyl CH and associated steric effects for **5**, and greater torsional-energy penalty for achieving the binding conformation for **1**.

Ultimately, **4** is the best inhibitor because it has the 2-pyridyl nitrogen and a negligible torsional-energy penalty, since the syn and anti forms are nearly isoenergetic (Figure 8), and it lacks the steric deficit of the oxazolyl C−H group. The torsional and steric penalties could also be reduced by enforcing planarity with fused ring systems replacing the biaryl ones. Thus, it is not surprising that the 4-aza-benzoxazolyl analogue has a similar K_i (0.0023 μM) as **4**.[17,18] The above analysis, which is based on the present structural and free-energy results, is supported by the generally good accord between the computed and observed binding data (Table 2). The observed and computed inhibitory orders are **4** ≫ **1**, **3**, **5** ≫ **2**. Quantitatively, the only significant discrepancy is that the MC/FEP results predict **4** to be even more potent than reported experimentally. Possible sources for the discrepancy include deficiencies in the partial charges for the oxadiazoles and the lack of protein backbone sampling in the MC simulations, which may disfavor the more sterically demanding oxazoles. It is also possible that the
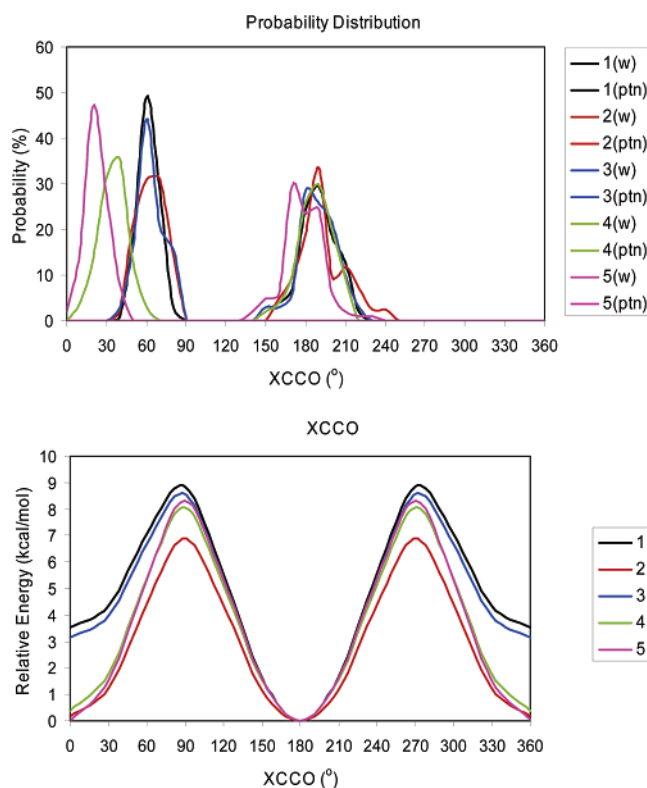

Figure 8. Energy profile in the gas phase (bottom) for the dihedral angle connecting the aromatic rings of **1**−**5**, NCCO for **1**, **3**, and **4** and CCCO for **2** and **5**, and (top) the probability distribution of sampling it in water (w) and the complexes (ptn).

experimental K_i for **4** was overestimated since the K_i and concentration of the enzyme (1−2 nM) in the assay are similar;[17] it is generally desirable to have the enzyme concentration considerably below the K_i to ensure equilibrium binding.

Conclusions

Fatty acid amide hydrolase (FAAH) is a serine hydrolase responsible for the degradation of anandamide and oleamide. Anandamide binds and activates the central (CB1) and peripheral (CB2) cannabinoid receptors as well as the vanilloid receptor (VR1) through which it is thought to exert its analgesic and cannabinoid effects. Oleamide was found to accumulate in the cerebrospinal fluid under conditions of sleep deprivation and to induce physiological sleep in animals. Recently, Boger and co-workers reported a potent, selective, and efficacious class of reversible α-ketoheterocycle inhibitors of FAAH that produced analgesia in animal models.[17,18] Striking aspects of the structure−activity data have been addressed through the present Monte Carlo simulations, which provided illuminating free-energy results and average computed structures. In particular, incorporation of pyridine at the C5 position of the 2-keto-oxazole and 2-keto-1,3,4-oxadiazole derivatives significantly boosts binding to FAAH due to formation of hydrogen-bonding interactions between the pyridyl nitrogen and Lys142 and Thr236. The results also show that substitution of oxazole by oxadiazole enhances activity not through additional hydrogen bonding with FAAH, but owing to a decrease in steric repulsion with Ile238 and to a lower conformational reorganization penalty, without the expense of a higher dehydration penalty. Despite the extra hydrogen bond acceptor site in an oxadiazole, the charges on the nitrogens of this ring are less negative than the charge on the oxazolyl nitrogen, and weaker hydrogen bonds with the solvent are formed. Finally, the reliability of the analysis is supported by the agreement between the experimental and calculated order of inhibitory strengths for **1**−**5**.

Supporting Information Available: Complete ref 36. This material is available free of charge via the Internet at http://pubs.acs.org.

JA055438J